by

Benjamin Grassian[1], Christopher Roman[2], Joe Warren [3], Dave Casagrande [4]

Prepared for submission to Limnology and Oceanography: Methods

[1]Ph.D. Candidate, Graduate School of Oceanography, The University of Rhode Island, Narragansett RI 02882. Email: bgrassian@gmail.com

[2]Professor of Oceanography, Graduate School of Oceanography, The University of Rhode Island, Narragansett RI 02882. Email: croman2@uri.edu

[3]Associate Professor, School of Marine and Atmospheric Sciences, Stony Brook University, Southampton, NY, 11968, USA. Email: jwarren@uri.edu

[4]Marine Development Engineer, Graduate School of Oceanography, The University of Rhode Island, Narragansett RI 02882. Email: dcasa@uri.edu

1 Abstract

Collecting detailed surveys of the environmental and biological distributions in the epi- and mesopelagic ocean is important for understanding the basic processes that govern these expansive habitats and influence the earth system at large. Common ocean sampling platforms (e.g. net systems, moored and shipboard sensors), are often unable to resolve marine biota at scales comparable to the variability associated with their own behaviour or that of their physical environment. Newer approaches using mobile robotic systems carrying multiple environmental sensors have enabled detailed interrogation of the fine and sub-mesoscale distribution of animals, and have provided more context for the water column structure. We integrated a dual-frequency broadband split-beam echosounder (Simrad EK80 with 70 and 200 kHz transducers) into the Wire Flyer profiling vehicle to achieve concurrent hydrographic and acoustic sections in the midwater environment (0-1000 meters) at novel scales. The Wire Flyer provides high-resolution repeat profiling (0-2.5 m/sec up and down velocity) within specified water column depth bands typically spanning 300-400m. This system can provide acoustic backscatter data at depths unavailable to shipboard surveys due to attenuation limits and can be operated in tandem with conventional shipboard echosounders to provide overlapping acoustic coverage with concurrent hydrographic sections. The side-looking transducer orientation, as opposed to the traditional vertically oriented arrangement on ships, samples orthogonal to the vehicle's profiling survey path and provides a direct measurement of animal distributions in the horizontal. The processed data have demonstrated the system's capacity to track migrating layers and resolve coherent biological patches and single targets in the horizontal, rising seafloor gas plumes, and scattering layer distributions tightly coupled to measured submesoscale features such as strong vertical oxygen gradients.

2 Introduction

The majority of the world's biomass resides within the mesopelagic region of the oceans [Kaartvedt et al., 2012, Irigoien et al., 2014, Proud et al., 2018]. The ability to measure deeper habitats is critical to understand a variety of fundamental dynamic physical and biological ocean processes. For example, the diverse habits of animals migrating into and out of these environments over daily cycles establishes the "biological pump" and underpins many of the ecological interactions in the open ocean [Bianchi et al., 2013, Benoit-Bird and McManus, 2014]. Overall, the biological and physical processes in this habitat are dynamic and vary on multiple temporal and spatial scales [Koslow et al., 2014, Sinclair and Stabeno, 2002]. This has made effective sampling of the mesopelagic difficult [Sutton et al., 2017], as traditional ocean sampling platforms (e.g. net systems, moored and shipboard sensors) are often unable to resolve marine biota at scales comparable to the variability in their physical environment. Furthermore, the biological and physical variability in the pelagic environment are

interconnected [Haury et al., 1978, Prairie et al., 2012]. Identifying the drivers of ecosystem processes in these habitats requires concurrent measurements of both of these, which is a sampling challenge beyond just the issue of resolution.

Traditional methods for surveying the pelagic ocean are limited in their ability to achieve these goals in terms of both scale and measurement diversity. Ship-based surveys using direct methods (e.g. nets) are severely restricted in their spatial and temporal resolutions, and indirect sensors (e.g. acoustics) can typically monitor the near-surface (i.e. epipelagic) regions over smaller spatial and time scales, but are limited in their ability to resolve smaller organisms (i.e. zooplankton) in the deeper parts of the water column (> 200 m) where acoustic attenuation and the beam geometry becomes limiting. Stationary sensor systems (e.g. moorings or buoys) can provide greater temporal resolution of these processes over longer time periods, but they are point samples and may alias the patchy nature of the region.

Towed rapid profiling instruments (e.g. the underway CTD (UCTD) [Rudnick and Klinke, 2007], SeaSoar [Pollard, 1986], moving vessel profiler (MVP) [Herman et al., 1998], or Wire Flyer [Roman et al., 2019]) can resolve the appropriate spatiotemporal scales and simultaneously record a number of complimentary measurements at depth, making these systems desirable for ecosystem exploration in the pelagic environment. The towed systems are typically operated in a "tow-yo" pattern, where the system is vertically profiled repetitiously while being towed horizontally with the ship, to produce the water column coverage necessary to evaluate vertical distributions and produce hydrographic sections of environmental data. These ancillary data (e.g. temperature, salinity and oxygen) taken at depth are useful and are typically lacking in shipboard acoustic surveys. Pairing these water column data collection systems with optical (e.g.[Cowen and Guigand, 2008]) or acoustic sensors allows for the analysis of biological distributions with respect to the detailed environmental sections.

Acoustic echosounders are widely used tools to measure the abundance and distribution of marine organisms, especially zooplankton and fish [Simmonds and MacLennan, 2008]. Acoustic sensors provide a way to remotely sample the marine environment at depths from the surface to 1000s of meters at very high temporal resolution (seconds). The effective range of acoustic systems however decreases with increasing frequency due to signal attenuation. Higher frequencies, greater than 38 kHz, are useful for measuring smaller organisms at low trophic levels such as crustacean zooplankton but are limited by range attenuation. Additionally, the ensonifed sample volume from ship-mounted systems increases with depth, which makes effective single target detection depth-dependant and more difficult for scatterers distributed in deeper regions [Diner, 2001]. For these reasons, the depth that vessel-based echosounders can effectively measure the abundance and distribution of marine organisms is limited. While lower frequency echosounders can measure acoustic backscatter throughout much of the mesopelagic region these systems will not resolve weaker scatterers in deep environments due to signal attenuation.

One solution to this range problem is to bring the echosounders to the scattering features of interest by lowering and/or towing them from a ship (e.g.

[Katz and Witzell Jr, 1979, Kloser, 1996, Wiebe et al., 2002, Lavery et al., 2019]). These systems often have incorporated multiple acoustic frequencies, environmental sensors and optical imagery to provide additional context to the acoustic data. Using coincident acoustic and imaging volumes has proven effective in confirming single targets, such as fish with swim bladders, and scattering strength estimates [Kloser et al., 2016]. When using vertically oriented transducers on towed vehicles, some of the acoustic data will still remain outside of the depth range where the vehicle has been profiling and collecting environmental data.

Vertically-lowered, acoustic profilers have been used to profile with side-looking (e.g. [Kloser et al., 2016]) and down-looking (e.g. [Marouchos et al., 2016, Haris et al., 2018]) transducers. Earlier vertically-profiling side-looking acoustic systems, specifically the Tracor Acoustic Profiling System (TAPS) and Multifrequency Acoustic Profiling System (MAPS), have provided bioacoustical data at up to megahertz frequencies with concurrent environmental measurements in the surface ocean [Holliday and Pieper, 1995]. These systems were configured to ensonify small sampling volumes (2-3 meters in horizontal range) in order to isolate recordings of zooplankton from larger scatters [Holliday et al., 1989]. Sonar information collected in the horizontal orientation has been analyzed from TAPS over short, meter scale ranges [Benoit-Bird and Au, 2003] where point sample data are typically derived instead of an analysis of backscatter returns over the full sampling ranges [Roman et al., 2001, McManus et al., 2003, Benoit-Bird et al., 2008].

Echosounders integrated into large [Fernandes et al., 2003, Patel et al., 2004, Scalabrin et al., 2009] and mid-size [Moline et al., 2015] autonomous underwater vehicles (AUVs) have also been effective at collecting data beyond the range of shipboard systems. By using dual frequencies these systems are able to provide animal discrimination at depths that are not achievable from shipboard systems (e.g. [Benoit-Bird et al., 2017]). Lower power gliders are also able to carry echosounders [Guihen et al., 2014, Suberg et al., 2014, Benoit-Bird et al., 2018]. Although somewhat constrained by power limitations, gliders fill a niche for multiday observations and have many operational advantages over more demanding ship and AUV operations.

In this paper we describe integrating a dual frequency (70 & 200 kHz) echosounder into the Wire Flyer towed vehicle [Roman et al., 2019]. The system utilizes the EK80 miniWBT echousounder in a similar manner as in [Benoit-Bird et al., 2018], but on a higher speed profiling vehicle with side-looking transducers. With the ability to quickly collect vertical profiles that are close in both time and space, the ability to study dynamic oceanographic (e.g. frontal systems, deep-sea vents, etc) or biological (e.g. animal zonation, deep scattering layer migration) processes can be improved. We present the integration of the acoustic system into the vehicle and sample data that demonstrate a new ability to resolve acoustic scattering with high resolution and coincident hydrographic data within the mesopelagic.

3 Materials and procedures

The Wire Flyer towed profiling system is able to provide rapid repeat profiling at high horizontal resolutions within a specified region of the water column [Roman et al., 2019] (Figure 1). The vehicle is autonomous and slides up and down a standard towed .322" CTD wire in an automatically controlled manner using the lift created by wing foils. A 2100 lb clump weight is towed below the lower profile depth to keep the tow wire taut, typically at 2-5 knots. The vehicle can achieve user specified up and down velocities (0-2.5 $\mathrm{m\,s^{-1}}$) while profiling down to 1000 meters. During deployments the vehicle is typically set to cover vertical bands of 300-400 meters positioned within the water column as needed. The Flyer is equipped with the suite of environmental sensors (Table 1) to produce detailed hydrographic sections of the water column with profiles that generally repeat with one kilometer spacing. A post processing routine written by the authors accounts for the cable shape and vehicle layback behind the ship to place the data at the proper location (e.g. Latitude, Longitude, depth).

3.1 Echosounder integration

The EK80 miniWBT (Simrad Kongsberg) [Demer et al., 2017] is integrated into the Wire Flyer as a stand-alone sensor packaged in its own 1500 meter rated pressure housing (Figure 2). The 200 kHz ES200-7CDK-split 7° and 70 kHz ES70-18CD, 18° transducers are inset into the syntactic foam flotation on the top of the Wire Flyer with the beams oriented level and pointing sideways. They are mostly flush with the side of the vehicle and bordered by a retaining bezel to minimize flow disturbance. Testing with thin plastic coverings to make a completely flush fairing did not cause a change in signal quality, providing some indication that the level of flow induced signal noise is low.

The EK80 miniWBT electronics were removed from the standard splash-proof rectangular case and repackaged in a 106 mm diameter and 260 mm long cylindrical housing. In this configuration the four acoustic channel cards required additional ribbon cables to plug into the main transceiver backplane. The Mission Controller and storage card is also packaged with the system. This repackaging allows the system to be removed from the Flyer for testing and also keeps it away from radiated electrical noise inside the Wire Flyer's main electronics housing. Each receiver card can be multiplexed to switch between two inputs, which provides eight total acoustic channels, four of which can be used at once. The EK80 receives power and has RS422 communications with the main Raspberry Pi vehicle computer. A switching circuit allows the communications lines to be routed to either the vehicle computer or outside the electronics housing via the deck cable so the EK Mission Planner software can have a dedicated connection from an external computer. Due to the noise sensitivity of the sonar [Benoit-Bird et al., 2018], power to the EK80 is filtered to achieve a roughly -50 dB noise reduction in the 75 kHz transducer band (Figure 3). We used an RC (resistor-capacitor) type filter with a capacitance multiplier to increase the filter's noise attenuation while avoiding a large voltage drop over

R1. The current through the resistor R1 is reduced by the T1 transistor gain, which is typically >100. Selection of T1 impacts the filter's effectiveness and efficiency. The high bandwidth, at least 1 MHz, allows the filter to remove noise up to that frequency while the low voltage drop increases efficiency. The capacitance multiplier is followed by a second RC stage with a small resistor, R2, to remove any high frequency noise passing through or introduced by the transistor. Figure 4 shows a comparison with and without the power filter. This evaluation was made by looking at the distribution of the return intensity as a function of range in a region of the water column relatively devoid of acoustic scatterers. Since the test was done while towing, it also provides an assessment of the lower detection limit that also incorporates flow noise due to the vehicle's motion. With the EK80 running at a nominal 6 W the endurance of the Wire Flyer with the 800 W h battery system is roughly 24 hours.

The EK80 mission files are planned and downloaded to the sonar prior to deployment. The mission plans are set up for a number of preset ensembles with transmit patterns for each frequency. A linux-based driver was written to interact with the EK80 via the RS422 communications interface. This driver connects to the EK80, sets the unit's time to match the vehicle's time and then sends the appropriate commands to transmit particular ensembles. The ensemble pattern is set as part of the Flyer's overall mission plan, and the driver changes the pinging pattern as needed during a mission. The EK80 is configured to output real-time volume backscattering strength (S_v) data for 20 range bins per ping. The driver records these messages as part of the standard data log and also flags other status messages indicating the state of the system. The logged S_v messages contain a timestamp from the EK80 that can be compared against the vehicle's time to correct for time drift within the sonar. These S_v data are also buffered in memory while operating and can be retrieved in snippets via the acoustic modem communications between the Wire Flyer and the ship side operator. This subsample of the data is useful to identify scattering aggregations and layers during a deployment. The full data are recorded on a large high speed USB flash drive in the EK80 electronics housing and retrieved for processing after a deployment.

The transmit sequence is typically configured to alternate frequencies in the up and down directions (Figure 5b) where the change in direction prompts the EK80 driver to switch the ping ensembles. In this pattern it is best to set the ensemble length longer than a single profile duration. If the ensemble completes, the unit will pause and require the driver to resend a command to continue pinging. This exchange will create a gap of a few seconds in the data. Changing frequencies also causes a 8-10 second gap when the unit switches the multiplexers to the other channel on each card before resuming pinging at the new frequency. This makes changing frequencies within a profile somewhat wasteful and is why we generally chose to switch channels between up and down casts. When the Flyer is in a hold depth mode of level flight the pinging is typically set to alternate frequencies, executing a fixed number of pings at each frequency before switching. Currently, we are unable to transmit both channels (700 and 200 kHz) simultaneously in split beam mode using the four available

transceiver channels. An additional switching circuit and rewiring could allow the 3-element 200 kHz ducer to run in split beam mode (3 channels) with the four elements of the 70 kHz ducer ganged together on a single channel as a single beam.

A unique aspect of the echosounder on this platform is the horizontal beam orientation, as opposed to the more traditional downward (or upward) transducers on ships and most other subsurface systems. An advantage of the side-looking arrangement is that the data are collected orthogonal to the movement of the platform, which creates an undulating ribbon of data as the vehicle moves forward and vertically. The size of the ensonified sampling volume is also constant across the profile depth and is coincident with the environmental measurements. In addition, the echosounder data is from a region that is physically separated from the vehicle and cable wake or bow-wave where animals are more likely to exhibit natural behaviors as opposed to an avoidance reaction. Several echosounders have been previously deployed in a horizontally forward or side-looking configuration arrangement (e.g. [Greene et al., 1998, Underwood et al., 2020, O'Driscoll et al., 2013, Easson et al., 2020]). One disadvantage of this geometry is that the majority of fisheries acoustics literature considers data from downward-looking system. Thus, the interpretation of volume backscatter or target strength data from these side-looking systems will be more complicated than traditional ship surveys. Additionally, scattering from elongated targets (e.g. fish and krill) is much more variable with rotation in the horizontal aspect than from the vertical perspective, further complicating the interpretation of the returned echoes.

3.2 Echosounder data processing

The sonar was configured in Frequency Modulated (FM) mode and fast ramping, with a pulse length of 2048 µs and a linear frequency sweep from 55-90 kHz and 185-255 kHz for the 70 and 200 kHz channels respectively. Simrad's broadband EK80 system outputs datagrams (.RAW file format) that encapsulate the system configuration and received acoustic information from both channels. To derive echocounting and echointegration values from the .RAW files, a software parser written in Matlab ingests the .RAW datagrams and calculates the Frequency Modulated (FM) pulse compressed and Continuous Wave (CW) versions of acoustic Power, Target Strength (TS) and Scattering Volume (S_v), and the angular positions, as described by [Andersen et al., 2021]. Processing the acoustic data in Matlab provides a means to merge it with Wire Flyer's location and depth data to create visualizations that are unavailable in standard tools like Echoview (https://echoview.com/). The FM pulse compressed data were calculated by match filtering with the time-reversed complex conjugate of the original transmit chirp that is twice filtered at receive and recreated using the frequency sweep, slope, and filter values stored in the .RAW datagrams. The match filter power was used to derive pulse compressed versions of S_v and TS, and CW (Continuous Wave) versions are derived using the raw power values and by appropriately scaling the effective pulse length. The CW values,

while inaccurate for the Frequency Modulated configuration, provide a dataset matching the mean volume backscatter strength calculated onboard the EK80 that is not match filtered and assumes only a single frequency, and are sufficient for on-the-fly mission adjustment and verification that the system is operating properly. The derived FM and CW echo integration and echocounting values are fused to the vehicle sensor information and stored in a data directory for post-processing.

The raw Sv data appeared to be dominated by the amplification of noise by the Time-Varying Gain (TVG) term, and a post-processing step was implemented to effectively 'flatten' the return over range. This post-processing step was applied differently for data collected before installation of the input power filter and for the higher SNR data collected following the power filter-installation (Figure 6). For the unfiltered data, the SV is detrended on a profile by profile (single up or downcasts) basis by averaging in the log domain all pings within that profile at depths unaffected by surface returns and median filtering the averaged signal to obtain a representative ping across range. This averaged ping is subtracted from each individual ping within that profile. The mean (Power/Sv/TS) value calculated in the log domain from all pings within the survey is then added back as an offset. This processing step also alleviated the non-stationary power trends observed over the duration of the dive in the earlier datasets, often where deep profile sections have an increased power/ noise floor relative to the shallow 0-400m sections. The higher SNR data collected after the installed power filter did not have the problem of a non-stationary noise floor/ power level across the duration of the dive, and these datasets were detrended as a single batch by averaging ping across all profiles at depths below 50m and adding back in an average value.

An additional post-processing step is performed to remove the roughly 1-4 pings that are interfered with every 30 seconds by the transmission from the acoustic modem used for vehicle and ship communications. The modem affected pings were mostly removed for the low SNR datasets with a median difference filter using the power values averaged from 50-100 m. In the higher SNR data after the power filter was implemented more scattering and single targets were resolved at farther ranges the median difference filter was less effective and we instead removed the interfered pings manually. In future deployments, the timestamp marking the modem transmissions will allow us to remove these pings excluding the data within a small time window around the modem transmit timing.

When the vehicle is near the surface, scattering from the air-water interface can be observed in the data. This is the triangular region of high intensity scattering seen in Figure 5a. The surface-reflected region is excluded during post processing, as shown in Figure 7. This section can be calculated from the transducer beam angle, and varies by several meters with sea surface state. A triangle extending from the far range at the surface is prescribed during processing and data within this region are automatically removed. An exclusion line from the full 100 m range at 50 meter depth back to the surface at a 5 m range is typically sufficient to remove the surface returns.

For data visualization, the processed Wire Flyer acoustic data can be range-averaged to render two-dimensional echograms similar to those obtained from shipboard systems 8. Since the range-averaged data occur along the vehicle's trajectory the coverage in the vertical is more sparse than a typical shipboard system, but the horizontal orientation enables better statistics at a given depth. The 2-dimensional echograms are useful for directly comparison to the simultaneously collected environmental data. The acoustic data can also be rendered in full as a 3-dimensional point cloud. For most of the 3-dimensional Wire Flyer data presented here the 3-d acoustic Scattering Volume pointclouds were overlaid on co-registered 2-d echograms obtained by a downward-looking echosounder systems at the surface on the ship. The Wire Flyer Scattering volume data was thresholded at a lower bound to only show returns indicative of single scatterers, scattering layers, and acoustically-detectable hydrographic features.

3.3 Acoustic scattering layers as recorded in the horizontal

Horizontally insonified scattering layers record different synoptic information than when seen from the vertical perspective (Figure 9). Compared to the vertical gradients, changes in backscatter intensity are typically smaller across the scattering layer horizontally, resulting in more constant backscatter over range. It was apparent when viewing the 3-dimensional data that the distribution of signal values in the data were dominated by either the amplification of the noise floor by the applied TVG curve in depopulated areas or relatively constant scattering intensities over range at scattering layers. For these reasons, we assumed constant scattering over range and detrended the data to a constant noise floor with the goal of obtaining the signal excess over range that is defined by the backscatter intensity, signal loss terms, and noise level. In the power data, the received backscatter decays logarithmically over the horizontal range due to spreading and absorption losses and the signal intensity falls below the noise floor at a certain distance (i.e. when the signal-to-noise ratio equals 0). When the signal loss terms are compensated by applying a TVG function (as is performed in the Sv and TS calculations), the noise floor is no longer fixed. By detrending the data over range (as described in the previous section), the signal excess is revealed with respect to a normalized noise floor. The balance between the scattering layer intensity and loss terms across the horizontal range explains the 'flame'-looking backscatter distribution seen in the 3-dimensional renders of the scattering layers. Within a layer the separation between the return scattering signal and the noise is greatest at short range, and then it decays with range due to the signal loss terms (i.e. spreading, absorption, and scattering) until the return signal is at the noise level. Denser scattering are detected over farther ranges (see Supplemental Information for more details). The standard approach to account for background noise is to estimate the noise floor for subset transmits sequences and to reject data along the noise floor as amplified by the applied TVG functions [De Robertis and Higginbottom, 2007]. This approach

is included in our processing, but the noise estimation for transmit sequences at dense scattering layers is not obtainable as the signal across the entire range is typically elevated by backscattering, and thus a noise level can only be assumed as an arbitrary upper threshold value. By deriving Sv data exceeding the noise floor, we improve the ability to detect and interpret scattering features from the full dataset.

3.4 Concurrent shipboard echosounding

Downward looking acoustic data were recorded using hull-mounted or tow-fish based downward looking echosounder systems during several Wire Flyer deployments to provide standard acoustic echograms for comparison and validation. A centerboard-mounted EK60 echosounder (operating at 38, 70, and 200 kHz) recorded concurrent CW acoustic data during deployments at the Costa Rica Margin in January 2019 from the R/V *Falkor*, and a dual-frequency (38 and 200 kHz ES60 echosounder was deployed off the starboard side of the R/V *Endeavor* using a small towfish during deployments in Baltimore Canyon in September 2019. The transducers were located at a depth of approximately 5m and 1m below the surface for the R/V *Falkor* EK60 and the towfish systems respectively. These backscatter data were processed using a combination of Echoview and Matlab scripts written by the authors. Surface and bottom exclusion zones were created to avoid noise from bubbles and bottom features and the background noise was removed following [De Robertis and Higginbottom, 2007]. Volume backscattering strength values were integrated into 25 or 50 m horizontal by 1 m vertical bins and then exported. The 25 x 1 m towfish echogram, used to show the cold seep in Section 4.4 was blurred using a Gaussian kernel after scaling the x-y echogram axes for the visualization. The downward looking acoustic data provided a ground truth and a comparison for the horizontally-beamed Wire Flyer data and were used to create the 3-dimensional data visualization products.

4 Assessment

The Wire Flyer and integrated echosounder have been used on three cruises, allowing us to investigate several different scenarios where the overlapping environmental and acoustic data provide insight into the mesopelagic habitat. We show examples of salient oceanographic phenomenon recorded by the Wire Flyer in the following sections: diel vertical migration, shallow water front, deep oxycline associated assemblages, and a gaseous cold seep plume. These represent several important biological and hydrographic features the Wire Flyer is uniquely suited to investigate. The DVM, shallow water front, and cold seep plume Wire Flyer data shown in the assessment sections were recorded from a single deployment in the Baltimore Canyon from the R/V *Endeavor* in September 2019 with concurrent downward echograms collected by a towfish. The full dataset from this deployment is shown previously in the 3-D 7 and range av-

eraged 8 examples. The second DVM dataset shown here was collected in the Costa Rica Margin from the R/V *Falkor* in January 2019, and the recording of the deep oxycline was collected in the Costa Rica Margin from the R/V *Atlantis* in Novemeber 2018.

4.1 Tracking diel migration

The massive Diel Vertical Migration (DVM) of animals at dawn and dusk is a near-ubiquitous biological phenomenon across the oceans that is well-studied using acoustic techniques. Shipboard acoustic observations of DVM around the globe has shown distinct regional heterogeneity in the timing and vertical redistribution of discrete scattering layers [Bianchi and Mislan, 2016]. Variability in these migration events helps support and modify the ecological interactions and biogeochemical exchanges between surface and deep communities. The dynamics of scattering layer migrations appear to vary among species and their life histories, with some animal assemblages settling at depths that are physiologically driven (constrained by the oxycline), determined by phototaxis (a fixed depth at a specific illumination intensity), and influenced by food availability and predator avoidance. To understand how the spatiotemporal aspects of migrating biological layers are influenced by the local environmental gradients requires concurrent hydrographic measurements recorded over the relevant depths and temporal scales. Additionally, observing migrating zooplankton layers requires high frequency acoustics that decay quickly over range and acoustic measurements that are not biased across the vertical sampling space. The importance of the massive mesopelagic fish community [Davison et al., 2013, St John et al., 2016] and its roles in the global carbon budget is a topic of growing interest [Robinson et al., 2010, Anderson and Tang, 2010].

We show here two examples of DVM events captured in detail by the Wire Flyer with concurrent shipboard and towfish acoustic perspectives from the R/V *Falkor* and R/V *Endeavor* respectively (Figure 10, 11). The Wire Flyer echograms show the higher frequency data collected in the scattering layers themselves, below the effective range of the shipboard measurements. Perhaps most importantly, the scattering layer features are similarly resolved and tracked at the surface by both systems suggesting that the differences in echosounder orientations (side vs down looking) is not problematic in terms of layer detection and tracking. Scattering layers that appear "patchy" in the along track aspect of the downward looking echogram have discrete "patchy" structures across the horizontal sampling range in the Wire Flyer data as well 11b. These findings help to confirm and describe the scales of heterogeneity of these scattering features. It is important to note that the apparent patchiness in the data could result from either variability in biomass, composition, or even the orientation of targets.

Most studies of mesopelagic deep scattering layers [Kaartvedt et al., 2012, D'elia et al., 2016, Boswell et al., 2020] rely on either one or two echosounder frequencies, typically 18 or 38 kHz. These frequencies allow recording of scattering layers at kilometer ranges from the surface. However, for most of the

water column only larger fishes or strongly-scattering gas-bearing (e.g. salps, siphonophores, fish with swim bladders) organisms are detected. We know that the mesopelagic community is exceptionally diverse [Sutton et al., 2017] and contains a variety of zooplankton and micronekton not well detected at these low frequencies (including the bristlemouth *Cyclothone* spp. which may be the most abundant vertebrate genus on the planet) [Nelson et al., 2016]. Use of the Wire Flyer to explore these habitats can provide novel insights into the characteristics and movements of migrating layers. For many of the resonant (i.e. swim-bladdered fish) scatterers, it is likely that the size or shape of their swimbladder will change as the animals move vertically in the water column. It is however incredibly difficult to get individual target strength measurements from these layers as they migrate with traditional sampling methods, but it would be possible to track a migrating layer by having the Flyer adjust its profiling accordingly to provide repeated measurements of individual scatterer characteristics over large depth ranges. AUV and glider-based echosounders could also collect these data, however their ability to track migrating layers vertically would be more challenging without guidance from other sensing systems.

4.2 Shallow water front

Frontal systems are common at shelf break environments where mixing between the epi- and meso-pelagic environment occurs [Gawarkiewicz and Chapman, 1992]. The passive aggregation of plankton at oceanic fronts creates unique physical environments that catalyse biological interactions. Frontal systems and submesoscale processes often support surface processes through nutrient enhancement [Denman and Powell, 1984] and coastal upwelling, promoting enhanced biological activity and an associated redirection of foraging and motile behaviors. The idea that the surface ocean may be dominated by ephemeral submesoscale circulation processes that passively drive the distribution of primary producers or actively enhance primary production is becoming more prominent [Pascual et al., 2017, Lévy et al., 2018, Rousselet et al., 2018]. High-resolution in situ assessments, alone and in combination with remote sensing and modelled information, have described nutrient distributions structured by filamentous submesoscale processes and the varying responses to both the physical and ecological aspects of these features among identified taxa [Luo et al., 2014, Hernández-Hernández et al., 2020, Siegelman et al., 2019].

The acoustic and environmental sections recorded by the Wire Flyer allow for near synoptic observation of the distribution of oceanic fronts and any associated redistribution of biological layers. In data recorded across a shallow water front across the Baltimore canyon from the R/V *Endeavor*, the division and aggregation of the biological layers is observed directly along the coherent edges of the front (Figure 12). The direct overlay of the environmental information and the biological layers provides observation of the coupling or lack of coupling between the environmental gradients imparted at the front and the distribution of biological layers. Turbulent features are visible in the environmental data across the front and corresponding alongtrack patchiness is observed in the 200

kHz scattering data.

Environmental [Houghton et al., 1986, Sundermeyer and Ledwell, 2001, Rienecker and Mooers, 1989] and biological [Yamamoto and Nishizawa, 1986, Ortner et al., 1978, Wiebe et al., 1992] measurements using towed vehicles or nets have been made across frontal zones for several decades. However, the vertical speeds of these towed samplers limits the horizontal spacing of the vertical profiles or the depth range which can be covered by the systems. The Wire Flyer platform produces data at a finer horizontal (order of a kilometer) and vertical (cm) scale than any other current sensor system and offers a novel look at the processes occurring at the fronts. In addition, other oceanographic frontal features such as warm and cold core rings could also be better resolved with the increased sampling capabilities of the Wire Flyer system.

4.3 Oxygen minimum zone vertical boundaries

Oxygen data collected at the Costa Rica Margin (8.96N, 84.31W) show the potential of the system to capture small scale structure within the Oxygen Minimum Zone (OMZ) and across the upper and lower oxycline boundaries. Deep horizontally-distributed physical features like the lower oxycline have acoustic scattering distributions which closely match the concurrently recorded vertical oxygen gradients (Figure 13). The lower oxycline measurements recorded by the Wire Flyer consistently show an associated scattering layer tightly coupled to very fine scale variations in the oxygen environment. The correlation between the scattering layer depth and features of the oxygen profile has been observed using CTD casts (e.g. [Netburn and Koslow, 2015, Klevjer et al., 2012]) but not with the level of detail seen here. This particular layer was persistent overnight and likely comprised of non-migrating animals whose depth is physiologically constrained at the lower oxycline [Wishner et al., 2013, Maas et al., 2014, Wishner et al., 2018]. As the distributions of the worlds OMZs are impacted in their extent and severity by ocean warming and climatic shifts, measurements capable of describing the settling depths and environments of migrating and non-migrating layers within the OMZ will prove valuable for discerning these animal habits as well as the anticipated impacts of the redistribution of the persistent oxygen boundaries.

4.4 Cold seep plume

Geologic features such as cold seeps support unique habitats [Åström et al., 2018] and chemical environments [Aloisi et al., 2002]. Measurements from cold seep gas plumes on the southern flank of the Baltimore Canyon just offshore of the New England shelf produced 3-dimensional sections of salient hydrographic features (Figure 14). The Wire Flyer sensor measurements provide a detailed recording of not only the plume itself, but how the plume dynamics evolves and imparts structure to the water column in space and time. The larger overall structure of the gaseous plume, as well as wandering smaller-scale filaments,

are well resolved in the 70 and 200 kHz data respectively. Compared to the 2-dimensional measurements from the surface-bound towfish, the Wire Flyer data constrains the totality of the feature and the finer athwartship structures. The inherent geometry of the Wire Flyer acoustic survey data allows for it to fully capture these features in a matter somewhat similar to water column imaging with multibeam sonar [Colbo et al., 2014] but with a level of detail not easily achieved from a surface vessel due to attenuation limits.

5 Discussion

The integration of side-looking broadband echosounders into a rapidly profiling vehicle provides several advantages over other sensing systems used today. However, there are several issues, some common to any mesopelagic sampler and some unique to the Wire Flyer platform, that need further investigation.

5.1 Echosounder calibration

A key component of any acoustic echosounder system is the calibration [Demer et al., 2015] which allows for comparison of data between different sites and systems and, in some cases, identification and discrimination of individual scatterers. Given the Wire Flyer configuration, in situ calibrations with a standard target positioned athwarthship of the vehicle would be very challenging to complete in most environments. However, the acoustic components can be separated from the Wire Flyer vehicle for an independent calibration using a hanging tethered sphere from a ship. A preliminary calibration provided poor coverage of the transducer surface (10 percent), but indicated moderate calibration values (i.e. mostly 1-4 dB differences between the raw and calibrated TS values) using the Simrad EK80 Software. Uncalibrated data from the Wire Flyer can also be compared with ship-board or tow-fish echosounders to look at the relative values of backscatter strength of near-surface scattering layers and aggregations. However, the direct comparison of TS or other scattering parameters between these two systems would need to account for the backscatter directivity of most marine organisms. Even without a calibration, the data collected are useful for the identification of distinct scattering features in the ocean and relative comparisons of backscattering levels from these features.

5.2 Pressure effects on transducers

While the transducers used in the system are rated to 1500 meters depth, the Wire Flyer profiling repeatedly and rapidly cycles the sensors over large pressure changes (e.g. 30-40 bar gradients over 4-5 mins). To our knowledge this is the most stress (in terms of depth changes per time) these standard echosounder transducers have been exposed to. In survey data collected before the installation of an input power filter in the EK80 sensor package, the 70 kHz power calculated for the individual transducer-elements varied over the course of a

dive. These increasing or decreasing per-element power trends were especially pronounced when operating below 300 m and transitioning from deep to shallow depth bands, which suggests that the vehicle operating depth (pressure) may be a factor. We do not yet have data collected below 350 m using the input-power filtered echosounder setup, and cannot yet discern if these varying per-element trends are still evident, however there was no divergence among element power unlike in prior shallow sections. For the affected data, profile-specific TVG detrending, as described in the methods, alleviated most of the observed variability over time. A dedicated per-element test and analysis will need to be conducted to discern the effects of rapid pressure cycling in the 0-1000 m depth range. Additional analysis of a pressure induced impedance changes may also indicate a contribution to the nonstationary noise floor in the acoustic measurements over the duration of the survey [Demer and Renfree, 2008].

5.3 Echosounder orientation and scatterer directivity

The majority of echosounder systems are deployed in near-vertical downward- (and to a lesser extent, upward-) looking configurations. Horizontally-oriented echosounders have been deployed on towed net systems and other platforms, but a major issue in the analysis of these side-looking data is whether the assumptions regarding target distribution, spacing, and other standards used to derive acoustic echo counting and echo integration quantities are still valid. The Wire Flyer acoustic data present an opportunity to reassess these assumptions for the horizontal-orientation perspective where a heterogeneous distribution of scatterers is observed within the beam pattern such as when profiling through scattering layers thinner than the beam width. Similarly, we have not yet derived frequency-dependent scatterer information (TS) for the broadband EK80 data, but we anticipate that standard scattering models will need to be modified (or re-calculated) for the geometry of this system.

As the Wire Flyer samples across dense scattering layers, the received backscatter signal is heavily attenuated over range. We assume the heavy attenuation of the acoustic returns while sampling within/ across dense scattering layers results in part from outgoing acoustic energy being scattered (in all directions) by the dense distributions of scatterers thus violating a key assumption in echo integration that most of the acoustic energy continues through scattering layers. If this assumption is violated, then analysis of our data may have to include multiple scattering theory as is done in the analysis of dense schools of fish where "shadow zones" exist below dense scattering aggregations. The loss of acoustic energy at the scattering layer depths is increased by the horizontal beam direction which samples a dense scatterer distribution across the entire signal, as opposed to downward looking systems which sample across the vertically compressed axis of these layers. If the signal loss due to enhanced extinction at dense scattering layers is better accounted for, quantification of scattering inhomogeneity or patchiness in the horizontal could be achieved, which remains an elusive measurement. Echo statistics [Chu and Stanton, 2010, Stanton et al., 2018] may be a useful way of investigating the scattering characteristics of these

layers. The influence of physical layering on the signal propagation could also contribute increased signal loss from the horizontal perspective and should be explored as well.

6 Summary

The results from this project demonstrate a new acoustic survey capability to acquire environmental and acoustic sections in the 0-1000m region of the ocean at novel resolutions. The side-looking transducer orientation samples orthogonal to the vehicle's profiling survey path and provides a unique three dimensional acoustic dataset with coincident environmental data. This unique survey perspective enables observation of the spatial and temporal aspects of biological and physical scattering processes within the ocean. The survey resolution provided by the Wire Flyer can resolve dynamic features that would be aliased or unresolved by other available survey platforms. The 3-dimensional acoustic data collected by the Wire Flyer has also proven capable of resolving biological patchiness and rising seafloor gas plumes across both the horizontal and vertical sampling perspectives. Collectively the contributions from this project help to further the technology-enabled exploration of ocean ecosystems and the vast but difficult to observe mesopelagic habitat.

Acknowledgements

The integration of the echosounder into the Wire Flyer vehicle was funded by the NOAA Office of Ocean Exploration under grant NA17OAR0110213. Fieldwork for the project was completed under NSF Ocean Sciences grant 1634559, Schmidt Ocean Institute cruise FK190106, and Rhode Island Endeavor Program cruise EN647. This work would not have been possible without the assistance of the captains and crew of the research vessels *Falkor*, *Endeavor*, and *Atlantis*. Todd Gregory of Gregory Designs completed the mechanical design work for the system integration. We thank two anonymous reviewers whose thoughtful comments substantially improved the quality of the manuscript.

Table 1: Wire Flyer sensors and parameters

Sensor	**Parameters**	**Sample rate**
SBE 49 FastCAT	Temperature, conductivty, depth	16 Hz
Aanderra 4831F optode	Oxygen	0.5 Hz
Wetlabs FLbb-2K	Chlorophyll-a, turbidity (700 nm)	1 Hz

7 Figures

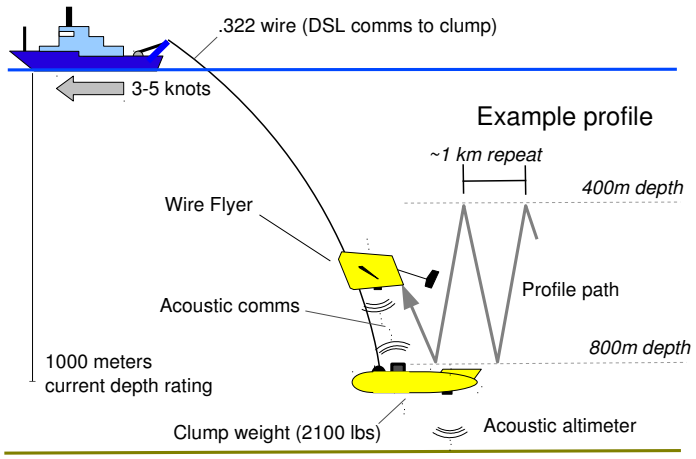

Figure 1: Wire Flyer towing diagram and sampling trajectory (reproduced from [Roman et al., 2019])

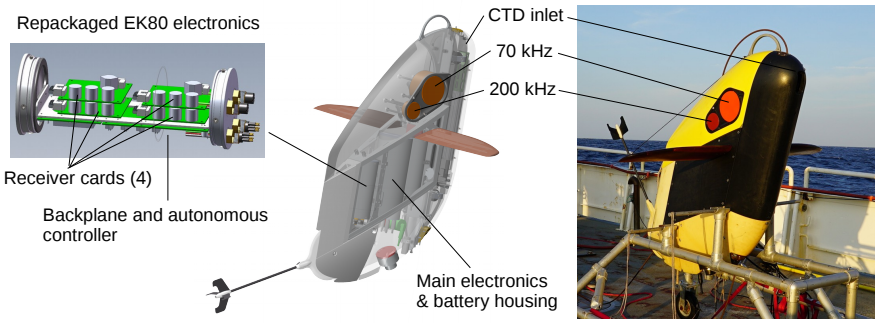

Figure 2: Wire Flyer mechanical details showing the repackaged EK80 electronics, the transducers inset into the foam flotation on the top of the vehicle and a photo of the Wire Flyer at sea. The oxygen sensor and fluorometer are mounted on the port side of the vehicle, out of view in this image.

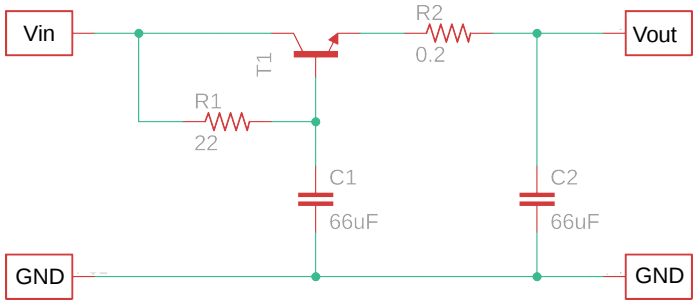

Figure 3: Schematic of the input power filter. Resistance values are in ohms.

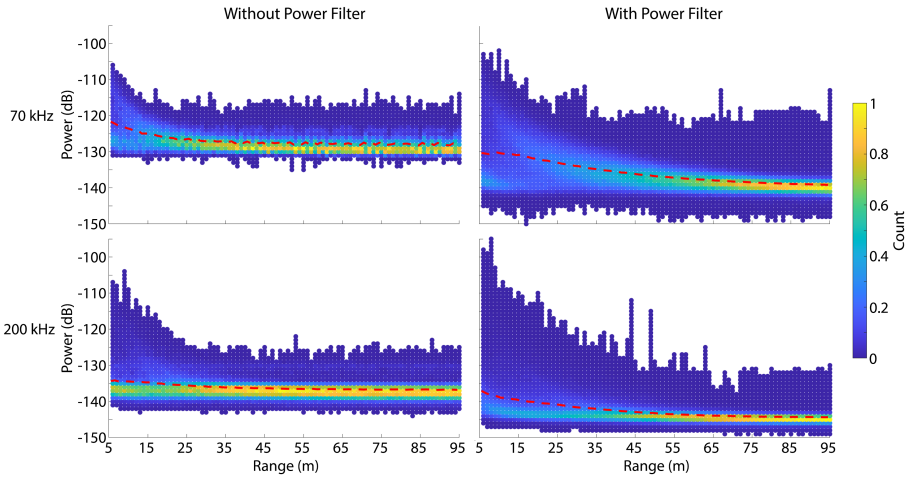

Figure 4: Comparison of the input power filtering. Colored histogram of the received signal levels over range for a section of the water column with little biomass. The dashed red line shows the mean received signal level. In both cases the high end of signal range is similar.

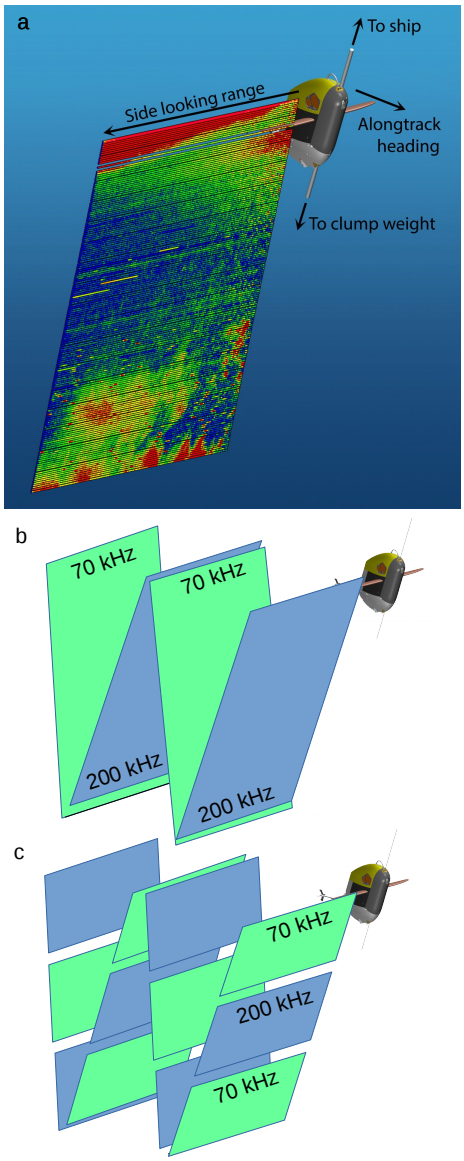

Figure 5: Wire Flyer side-looking acoustic survey. (**a**) Sample of detailed side looking 70 kHz data showing surface-reflected returns and a scattering layer near the surface and a gas plume with apparent horizontal structure at depth. (**b**) The typical sampling pattern alternating frequencies on the up and down profiles. (**c**) Alternating pings by depth or time within a profile.

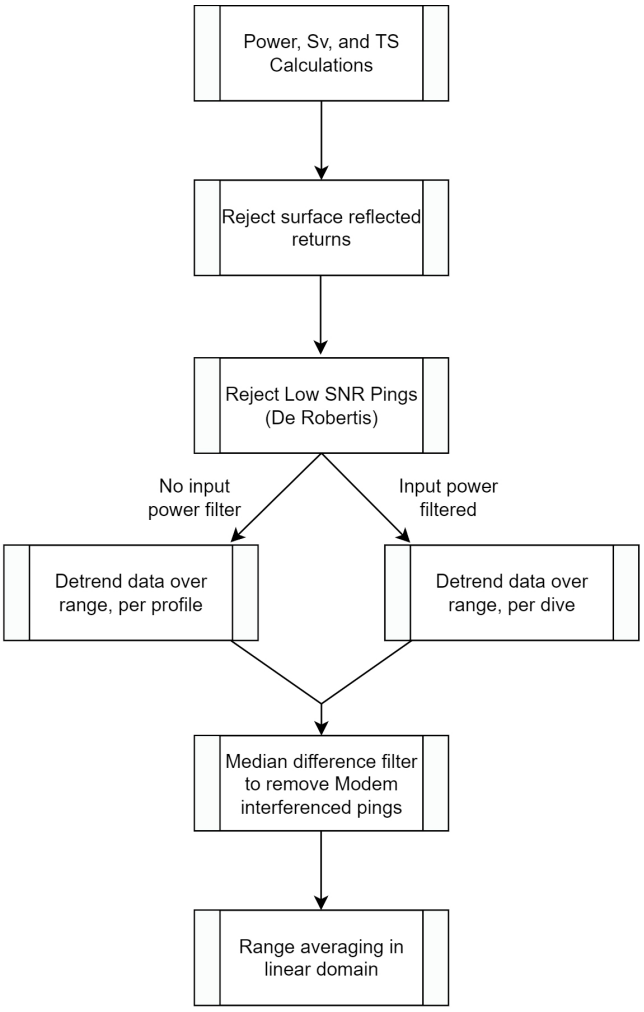

Figure 6: Process diagram outlining the Wire Flyer acoustic processing pipeline. De Robertis refers to the noise rejection method described in [De Robertis and Higginbottom, 2007].

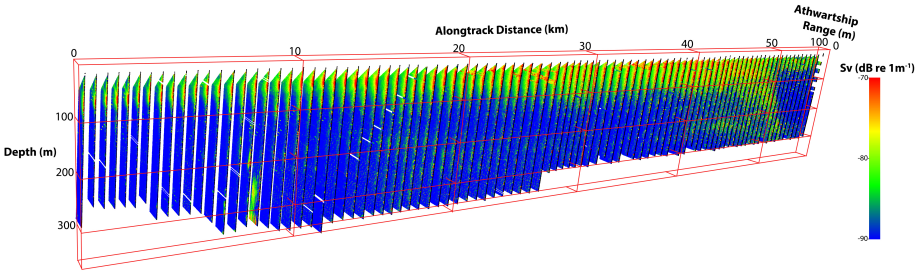

Figure 7: 3D rendering of the Wire Flyer acoustic data showing side-looking acoustic data "unwrapped" along the vehicle path. Data collected on the R/V *Endeavor* from 23 Sept 2019 23:13 - 24 Sept 2019 11:56 (UTC) in the Baltimore Canyon (37.99, -73.87 Lat, Lon)

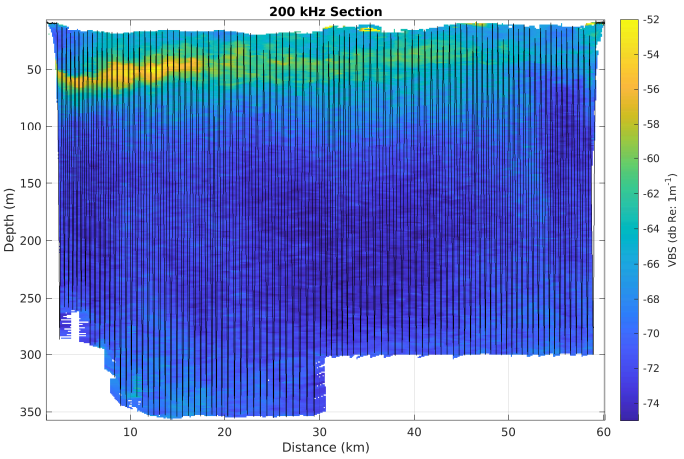

(a) Flyer 200 kHz

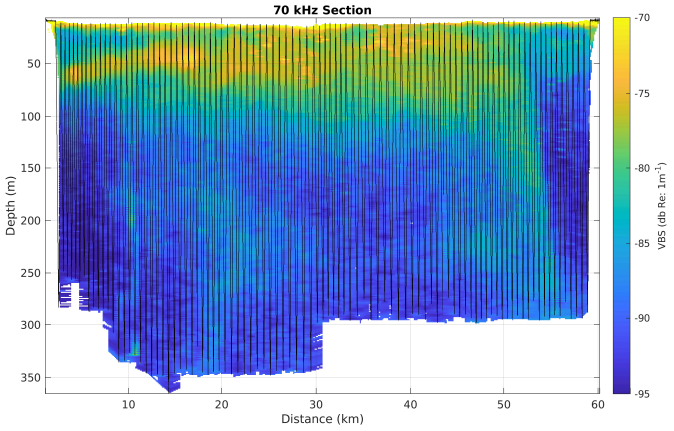

(b) Flyer 70 kHz

Figure 8: Section plots showing Scattering Volume averaged between 5 and 35 meters range and the Wire Flyer survey path for the a) 200 kHz and b) 70 kHz profiles. Data collected on the R/V *Endeavor* 23 Sept 2019 23:13 - 24 Sept 2019 11:56 UTC in the Baltimore Canyon 37.99 Lat -73.87 Lon.

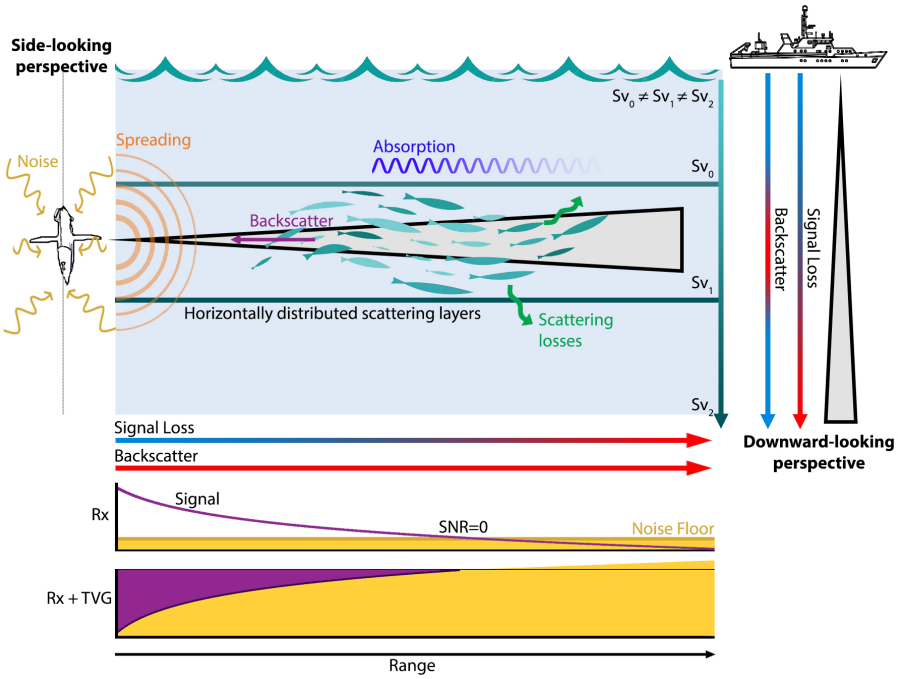

Figure 9: Schematic illustrating the fate of a side looking ping. The signal is attenuated over range due to the transmission loss terms and falls below the noise floor at range. The TVG amplification of the received backscatter signal, to compensate for the transmission loss, generates a non-fixed noise floor that increases over range.

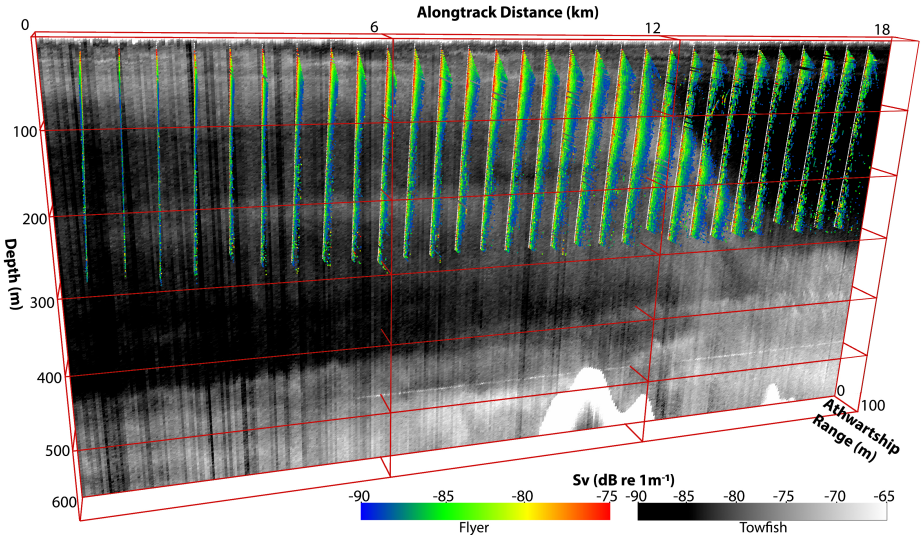

(a) Towfish 38 and Wire Flyer 70 kHz

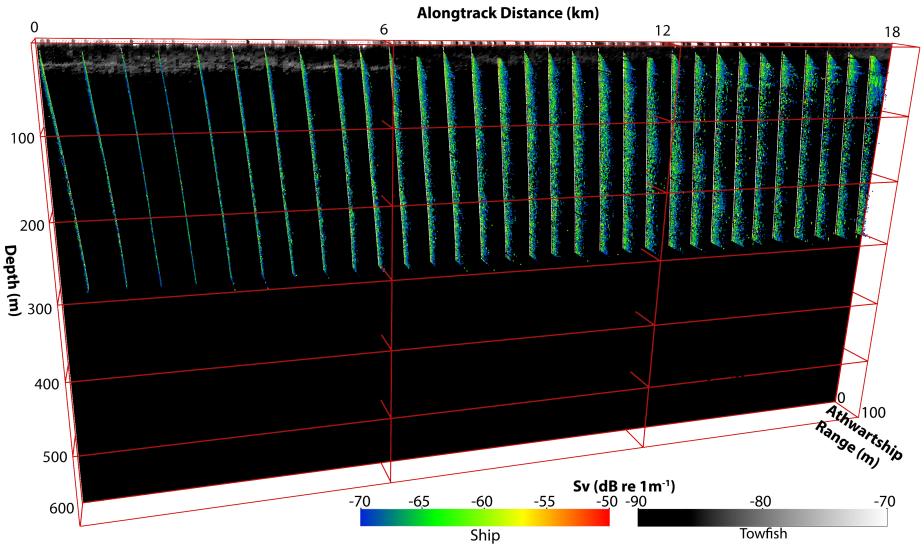

(b) Towfish 200 and Wire Flyer 200 kHz

Figure 10: Downward diel migration near the Baltimore Canyon (38.020 Lat -73.862 Lon) from the R/V *Endeavor*, 24 Sept 2019 07:22 - 24 Sept 2019 11:34 UTC. (**a** Shipboard 38 kHz shown in gray with the side looking Wire Flyer 70 kHz data shown in color and thresholded at the lower end. (**b**) 200 kHz Wire Flyer and shipboard data.

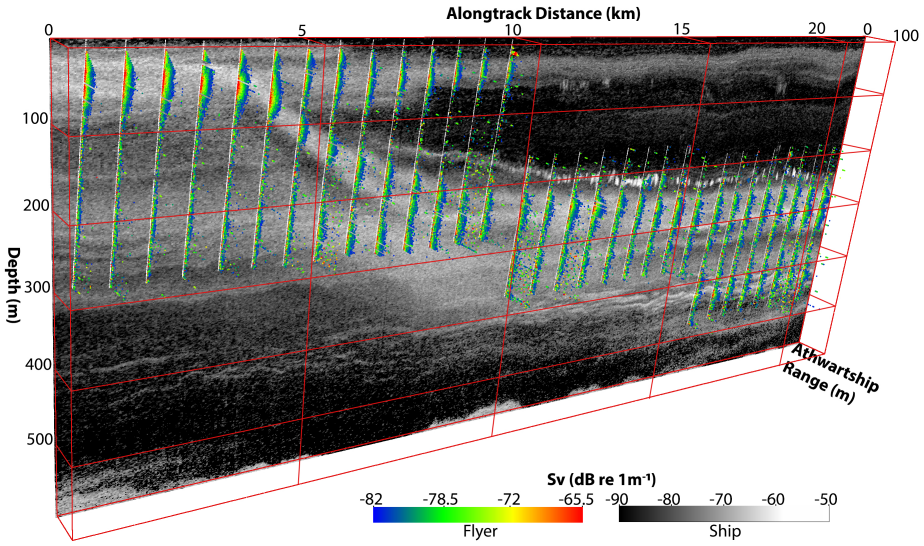

(a) Shipboard and Wire Flyer 70 kHz

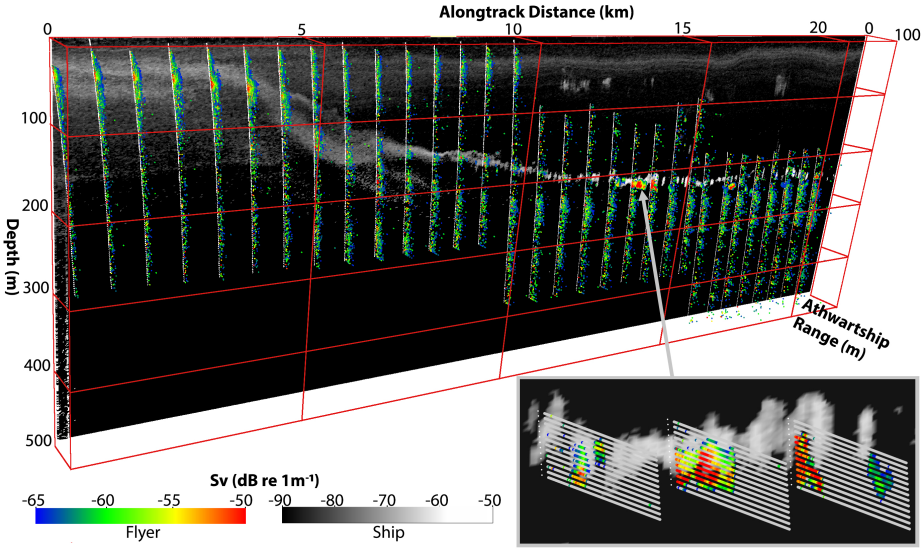

(b) Shipboard and Wire Flyer 200 kHz

Figure 11: Downward diel migration at the Costa Rica Margin from the R/V *Falkor*, 24 Jan 2019 10:58 - 14:32, 8.536 Lat -85.441 Lon . (**a**) Shipboard 38 kHz shown in gray with the side looking Wire Flyer 70 kHz data shown in color and thresholded at the lower end. (**b**) 200 kHz Wire Flyer and shipboard data. Inset highlights patchy scattering features.

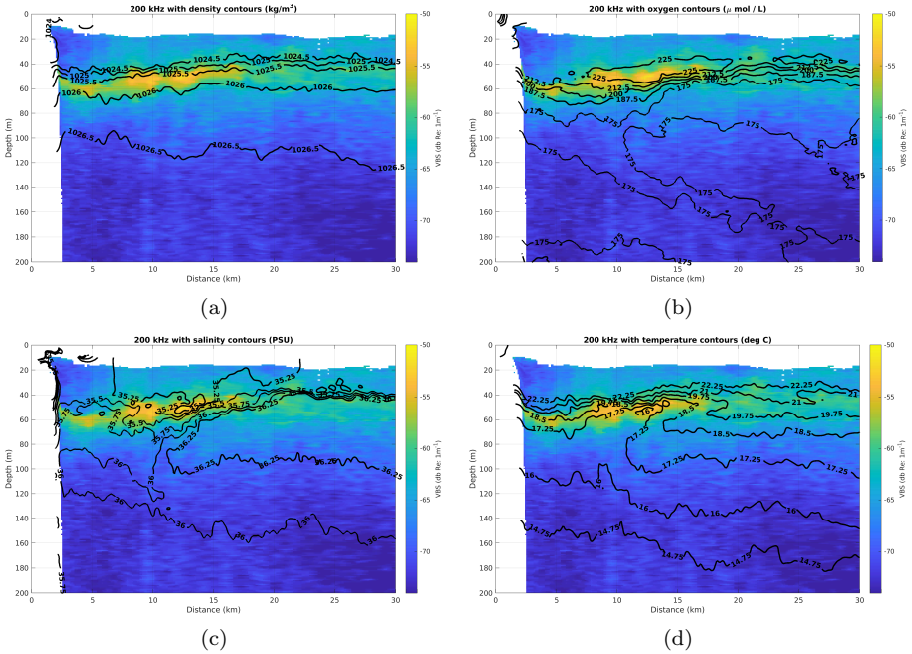

Figure 12: Transect recording a frontal feature across the Baltimore Canyon from the R/V *Endeavor*, 37.989 Lat -73.892 - 38.123 Lat -73.64, 24 Sept 2019 23:13 - 24 Sept 2019 05:03 UTC. Overlays of (**a**) density, (**b**) oxygen, (**c**) salinity, and (**d**) temperature all show good agreement with the concentration in acoustic scattering.

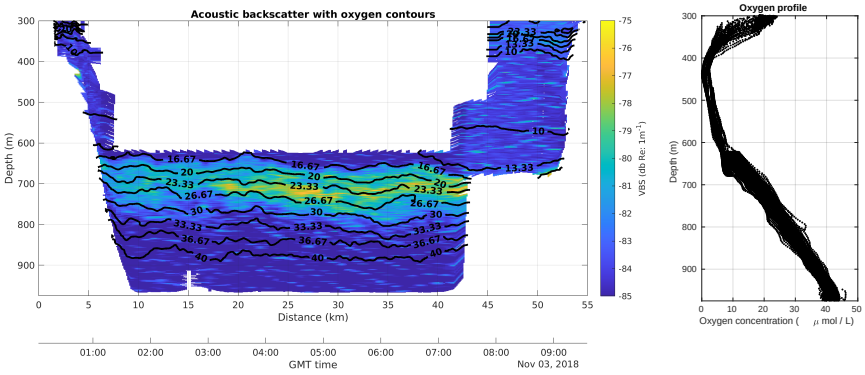

(a) (b)

Figure 13: Wire Flyer transect at the lower oxycline in the Costa Rica Margin (GMT-6) from the R/V *Atlantis*, 8.845, Lat 84.210 Lon - 9.050 Lat, -84.538 Lon. (**a**) 70 kHz Wire Flyer acoustic data from with the oxygen concentration contours overlaid. (**b**) Scatter plot of oxygen measurements from all of the Wire Flyer profiles indicating the minimum depth and variability amongst the profiles over the length of the transect. These data were collected prior to the final power filter, so the overall signal range is limited by the higher noise floor.

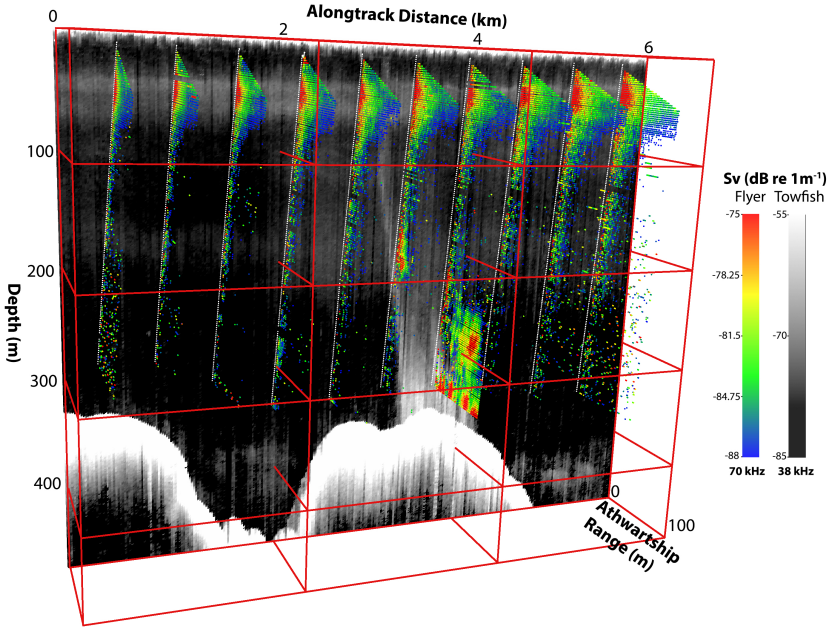

(a)

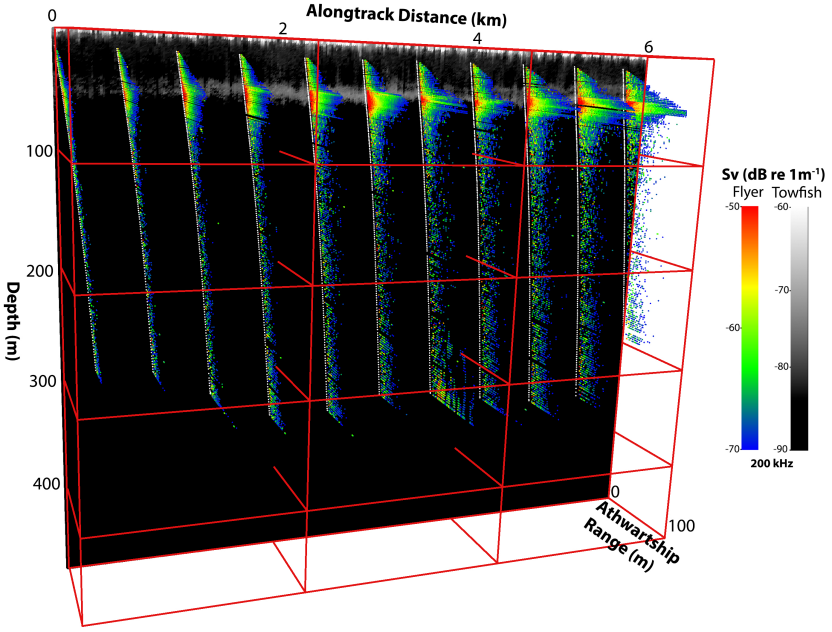

(b)

Figure 14: Wire Flyer acoustic transect at a cold seep plume on the southern flank of the Baltimore Canyon (38.050, -73.825, Lat Lon). Data collected from the R/V *Endeavor* 24 Sept 2019 00:23 - 01:42 UTC.

References

[Aloisi et al., 2002] Aloisi, G., Bouloubassi, I., Heijs, S. K., Pancost, R. D., Pierre, C., Damsté, J. S. S., Gottschal, J. C., Forney, L. J., and Rouchy, J.-M. (2002). Ch4-consuming microorganisms and the formation of carbonate crusts at cold seeps. *Earth and Planetary Science Letters*, 203(1):195–203.

[Andersen et al., 2021] Andersen, L. N., Chu, D., Heimvoll, H., Korneliussen, R., Macaulay, G. J., and Ona, E. (2021). Quantitative processing of broadband data as implemented in a scientific splitbeam echosounder. *arXiv preprint arXiv:2104.07248*.

[Anderson and Tang, 2010] Anderson, T. R. and Tang, K. W. (2010). Carbon cycling and poc turnover in the mesopelagic zone of the ocean: Insights from a simple model. *Deep Sea Research Part II: Topical Studies in Oceanography*, 57(16):1581–1592.

[Åström et al., 2018] Åström, E. K., Carroll, M. L., Ambrose Jr, W. G., Sen, A., Silyakova, A., and Carroll, J. (2018). Methane cold seeps as biological oases in the high-arctic deep sea. *Limnology and Oceanography*, 63(S1):S209–S231.

[Benoit-Bird et al., 2018] Benoit-Bird, K., Waluk, C., Welch, P., A. Barth, J., Wangen, I., McGill, P., Okuda, C., Hollinger, G., Sato, M., and Mccammon, S. (2018). Equipping an underwater glider with a new echosounder to explore ocean ecosystems. *Limnology and oceanography, methods*.

[Benoit-Bird and Au, 2003] Benoit-Bird, K. J. and Au, W. W. (2003). Echo strength and density structure of hawaiian mesopelagic boundary community patches. *The Journal of the Acoustical Society of America*, 114(4):1888–1897.

[Benoit-Bird and McManus, 2014] Benoit-Bird, K. J. and McManus, M. A. (2014). A critical time window for organismal interactions in a pelagic ecosystem. *PLoS One*, 9(5):e97763.

[Benoit-Bird et al., 2017] Benoit-Bird, K. J., Moline, M. A., and Southall, B. L. (2017). Prey in oceanic sound scattering layers organize to get a little help from their friends. *Limnology and Oceanography*, 62(6):2788–2798.

[Benoit-Bird et al., 2008] Benoit-Bird, K. J., Zirbel, M. J., and McManus, M. A. (2008). Diel variation of zooplankton distributions in hawaiian waters favors horizontal diel migration by midwater micronekton. *Marine Ecology Progress Series*, 367:109–123.

[Bianchi and Mislan, 2016] Bianchi, D. and Mislan, K. (2016). Global patterns of diel vertical migration times and velocities from acoustic data. *Limnology and Oceanography*, 61(1):353–364.

[Bianchi et al., 2013] Bianchi, D., Stock, C., Galbraith, E. D., and Sarmiento, J. L. (2013). Diel vertical migration: Ecological controls and impacts on the biological pump in a one-dimensional ocean model. *Global Biogeochemical Cycles*, 27(2):478–491.

[Boswell et al., 2020] Boswell, K. M., D'Elia, M., Johnston, M. W., Mohan, J. A., Warren, J. D., Wells, R., and Sutton, T. T. (2020). Oceanographic structure and light levels drive patterns of sound scattering layers in a low-latitude oceanic system. *Frontiers in Marine Science*, 7:51.

[Chu and Stanton, 2010] Chu, D. and Stanton, T. K. (2010). Statistics of echoes from a directional sonar beam insonifying finite numbers of single scatterers and patches of scatterers. *IEEE journal of oceanic engineering*, 35(2):267–277.

[Colbo et al., 2014] Colbo, K., Ross, T., Brown, C., and Weber, T. (2014). A review of oceanographic applications of water column data from multibeam echosounders. *Estuarine, Coastal and Shelf Science*, 145:41–56.

[Cowen and Guigand, 2008] Cowen, R. K. and Guigand, C. M. (2008). In situ ichthyoplankton imaging system (isiis): system design and preliminary results. *Limnology and Oceanography: Methods*, 6(2):126–132.

[Davison et al., 2013] Davison, P., Checkley Jr, D., Koslow, J., and Barlow, J. (2013). Carbon export mediated by mesopelagic fishes in the northeast pacific ocean. *Progress in Oceanography*, 116:14–30.

[De Robertis and Higginbottom, 2007] De Robertis, A. and Higginbottom, I. (2007). A post-processing technique to estimate the signal-to-noise ratio and remove echosounder background noise. *ICES Journal of Marine Science*, 64(6):1282–1291.

[D'elia et al., 2016] D'elia, M., Warren, J. D., Rodriguez-Pinto, I., Sutton, T. T., Cook, A., and Boswell, K. M. (2016). Diel variation in the vertical distribution of deep-water scattering layers in the gulf of mexico. *Deep Sea Research Part I: Oceanographic Research Papers*, 115:91–102.

[Demer et al., 2017] Demer, D., Andersen, L., Bassett, C., Berger, L., Chu, D., Condiotty, J., and Cutter, G. (2017). Evaluation of a wideband echosounder for fisheries and marine ecosystem science. *ICES Cooperative Research Report*, (336).

[Demer et al., 2015] Demer, D. A., Berger, L., Bernasconi, M., Bethke, E., Boswell, K., Chu, D., Domokos, R., Dunford, A., Fassler, S., Gauthier, S., et al. (2015). Calibration of acoustic instruments.

[Demer and Renfree, 2008] Demer, D. A. and Renfree, J. S. (2008). Variations in echosounder–transducer performance with water temperature. *ICES Journal of Marine Science*, 65(6):1021–1035.

[Denman and Powell, 1984] Denman, K. L. and Powell, T. M. (1984). Effects of physical processes on planktonic ecosystems in the coastal ocean. *Oceanogr. Mar. Biol. Ann. Rev*, 22:125–168.

[Diner, 2001] Diner, N. (2001). Correction on school geometry and density: approach based on acoustic image simulation. *Aquatic Living Resources*, 14(4):211–222.

[Easson et al., 2020] Easson, C. G., Boswell, K. M., Tucker, N., Warren, J. D., and Lopez, J. V. (2020). Combined edna and acoustic analysis reflects diel vertical migration of mixed consortia in the gulf of mexico. *Frontiers in Marine Science*.

[Fernandes et al., 2003] Fernandes, P. G., Stevenson, P., Brierley, A. S., Armstrong, F., and Simmonds, E. J. (2003). Autonomous underwater vehicles: future platforms for fisheries acoustics. *ICES Journal of Marine Science*, 60(3):684–691.

[Gawarkiewicz and Chapman, 1992] Gawarkiewicz, G. and Chapman, D. C. (1992). The role of stratification in the formation and maintenance of shelf-break fronts. *Journal of Physical Oceanography*, 22(7):753–772.

[Greene et al., 1998] Greene, C. H., Wiebe, P. H., Pershing, A. J., Gal, G., Popp, J. M., Copley, N. J., Austin, T. C., Bradley, A. M., Goldsborough, R. G., Dawson, J., et al. (1998). Assessing the distribution and abundance of zooplankton: a comparison of acoustic and net-sampling methods with d-bad mocness. *Deep Sea Research Part II: Topical Studies in Oceanography*, 45(7):1219–1237.

[Guihen et al., 2014] Guihen, D., Fielding, S., Murphy, E. J., Heywood, K. J., and Griffiths, G. (2014). An assessment of the use of ocean gliders to undertake acoustic measurements of zooplankton: the distribution and density of antarctic krill (euphausia superba) in the weddell sea. *Limnology and Oceanography: Methods*, 12(6):373–389.

[Haris et al., 2018] Haris, K., Kloser, R. J., Ryan, T. E., and Malan, J. (2018). Deep-water calibration of echosounders used for biomass surveys and species identification. *ICES Journal of Marine Science*, 75(3):1117–1130.

[Haury et al., 1978] Haury, L., McGowan, J., and Wiebe, P. (1978). Patterns and processes in the time-space scales of plankton distributions. In *Spatial pattern in plankton communities*, pages 277–327. Springer.

[Herman et al., 1998] Herman, A. W., Beanlands, B., Chin-Yee, M., Furlong, A., Snow, J., Young, S., and Phillips, T. (1998). The Moving Vessel Profiler (MVP): In-situ sampling of plankton and physical parameters at 12 kts and the integration of a new laser/optical plankton counter. In *Proceedings of Oceanology International*, volume 102, pages 123–135.

[Hernández-Hernández et al., 2020] Hernández-Hernández, N., Arístegui, J., Montero, M. F., Velasco-Senovilla, E., Baltar, F., Marrero-Díaz, Á., Martínez-Marrero, A., and Rodríguez-Santana, Á. (2020). Drivers of plankton distribution across mesoscale eddies at submesoscale range. *Frontiers in Marine Science*, 7:667.

[Holliday and Pieper, 1995] Holliday, D. and Pieper, R. (1995). Bioacoustical oceanography at high frequencies. *ICES Journal of marine Science*, 52(3-4):279–296.

[Holliday et al., 1989] Holliday, D., Pieper, R., and Kleppel, G. (1989). Determination of zooplankton size and distribution with multifrequency acoustic technology. *ICES Journal of Marine Science*, 46(1):52–61.

[Houghton et al., 1986] Houghton, R. W., Olson, D. B., and Celone, P. J. (1986). Observation of an anticyclonic eddy near the continental shelf break south of new england. *Journal of Physical Oceanography*, 16(1):60–71.

[Irigoien et al., 2014] Irigoien, X., Klevjer, T. A., Røstad, A., Martinez, U., Boyra, G., Acuña, J. L., Bode, A., Echevarria, F., Gonzalez-Gordillo, J. I., Hernandez-Leon, S., et al. (2014). Large mesopelagic fishes biomass and trophic efficiency in the open ocean. *Nature communications*, 5(1):1–10.

[Kaartvedt et al., 2012] Kaartvedt, S., Staby, A., and Aksnes, D. L. (2012). Efficient trawl avoidance by mesopelagic fishes causes large underestimation of their biomass. *Marine Ecology Progress Series*, 456:1–6.

[Katz and Witzell Jr, 1979] Katz, E. J. and Witzell Jr, W. E. (1979). A depth controlled tow system for hydrographic and current measurements with applications. *Deep Sea Research Part A. Oceanographic Research Papers*, 26(5):579–596.

[Klevjer et al., 2012] Klevjer, T., Torres, D., and Kaartvedt, S. (2012). Distribution and diel vertical movements of mesopelagic scattering layers in the red sea. *Marine Biology*, 159.

[Kloser, 1996] Kloser, R. J. (1996). Improved precision of acoustic surveys of benthopelagic fish by means of a deep-towed transducer. *ICES Journal of Marine Science*, 53(2):407–413.

[Kloser et al., 2016] Kloser, R. J., Ryan, T. E., Keith, G., and Gershwin, L. (2016). Deep-scattering layer, gas-bladder density, and size estimates using a two-frequency acoustic and optical probe. *ICES Journal of Marine Science*, 73(8):2037–2048.

[Koslow et al., 2014] Koslow, J. A., Davison, P., Lara-Lopez, A., and Ohman, M. D. (2014). Epipelagic and mesopelagic fishes in the southern california current system: Ecological interactions and oceanographic influences on their abundance. *Journal of Marine Systems*, 138:20–28.

[Lavery et al., 2019] Lavery, A. C., Stanton, T. K., Jech, J. M., and Wiebe, P. (2019). An advanced sensor platform for acoustic quantification of the ocean twilight zone. *The Journal of the Acoustical Society of America*, 145(3):1653–1653.

[Lévy et al., 2018] Lévy, M., Franks, P. J., and Smith, K. S. (2018). The role of submesoscale currents in structuring marine ecosystems. *Nature communications*, 9(1):1–16.

[Luo et al., 2014] Luo, J. Y., Grassian, B., Tang, D., Irisson, J.-O., Greer, A. T., Guigand, C. M., McClatchie, S., and Cowen, R. K. (2014). Environmental drivers of the fine-scale distribution of a gelatinous zooplankton community across a mesoscale front. *Marine Ecology Progress Series*, 510:129–149.

[Maas et al., 2014] Maas, A. E., Frazar, S. L., Outram, D. M., Seibel, B. A., and Wishner, K. F. (2014). Fine-scale vertical distribution of macroplankton and micronekton in the eastern tropical north pacific in association with an oxygen minimum zone. *Journal of plankton research*, 36(6):1557–1575.

[Marouchos et al., 2016] Marouchos, A., Sherlock, M., Kloser, R. J., Ryan, T., and Cordell, J. (2016). A profiling acoustic and optical system (paos) for pelagic studies; prototype development and testing. *OCEANS 2016 - Shanghai*, pages 1–6.

[McManus et al., 2003] McManus, M., Alldredge, A., Barnard, A., Boss, E., Case, J., Cowles, T., Donaghay, P., Eisner, L., Gifford, D., Greenlaw, C., et al. (2003). Characteristics, distribution and persistence of thin layers over a 48 hour period. *Marine Ecology Progress Series*, 261:1–19.

[Moline et al., 2015] Moline, M. A., Benoit-Bird, K., O'Gorman, D., and Robbins, I. C. (2015). Integration of scientific echo sounders with an adaptable autonomous vehicle to extend our understanding of animals from the surface to the bathypelagic. *Journal of Atmospheric and Oceanic Technology*, 32(11):2173–2186.

[Nelson et al., 2016] Nelson, J. S., Grande, T. C., and Wilson, M. V. (2016). *Fishes of the World*. John Wiley and Sons.

[Netburn and Koslow, 2015] Netburn, A. N. and Koslow, J. A. (2015). Dissolved oxygen as a constraint on daytime deep scattering layer depth in the southern california current ecosystem. *Deep Sea Research Part I: Oceanographic Research Papers*, 104:149 – 158.

[Ortner et al., 1978] Ortner, P. B., Wiebe, P. H., Haury, L., and Boyd, S. (1978). Variability in zooplankton biomass distribution in the northern sargasso sea: the contribution of gulf stream cold core rings. *Fishery Bulletin*, 76(2):323–334.

[O'Driscoll et al., 2013] O'Driscoll, R., Oeffner, J., Ross, O., Dunford, A., and McMillan, P. (2013). Pilot acoustic survey for jack mackerel on the west coast new zealand (jma7). *New Zealand Fisheries Assessment Report*, 1:1–53.

[Pascual et al., 2017] Pascual, A., Ruiz, S., Olita, A., Troupin, C., Claret, M., Casas, B., Mourre, B., Poulain, P.-M., Tovar-Sanchez, A., Capet, A., et al. (2017). A multiplatform experiment to unravel meso-and submesoscale processes in an intense front (alborex). *Frontiers in Marine Science*, 4:39.

[Patel et al., 2004] Patel, R., Handegard, N. O., and Godø, O. R. (2004). Behaviour of herring (clupea harengus l.) towards an approaching autonomous underwater vehicle. *ICES Journal of Marine Science*, 61(7):1044–1049.

[Pollard, 1986] Pollard, R. (1986). Frontal surveys with a towed profiling conductivity/temperature/depth measurement package (SeaSoar). *Nature*, 323:433–435.

[Prairie et al., 2012] Prairie, J. C., Sutherland, K. R., Nickols, K. J., and Kaltenberg, A. M. (2012). Biophysical interactions in the plankton: A cross-scale review. *Limnology and Oceanography: Fluids and Environments*, 2(1):121–145.

[Proud et al., 2018] Proud, R., Handegard, N. O., Kloser, R. J., Cox, M. J., and Brierley, A. S. (2018). From siphonophores to deep scattering layers: uncertainty ranges for the estimation of global mesopelagic fish biomass. *ICES Journal of Marine Science*, 76(3):718–733.

[Rienecker and Mooers, 1989] Rienecker, M. M. and Mooers, C. N. (1989). Mesoscale eddies, jets, and fronts off point arena, california, july 1986. *Journal of Geophysical Research: Oceans*, 94(C9):12555–12569.

[Robinson et al., 2010] Robinson, C., Steinberg, D. K., Anderson, T. R., Arístegui, J., Carlson, C. A., Frost, J. R., Ghiglione, J.-F., Hernández-León, S., Jackson, G. A., Koppelmann, R., et al. (2010). Mesopelagic zone ecology and biogeochemistry–a synthesis. *Deep Sea Research Part II: Topical Studies in Oceanography*, 57(16):1504–1518.

[Roman et al., 2019] Roman, C., Ullman, D. S., Hebert, D., and Licht, S. (2019). The Wire Flyer Towed Profiling System. *Journal of Atmospheric and Oceanic Technology*, 36(2):161–182.

[Roman et al., 2001] Roman, M. R., Holliday, D. V., and Sanford, L. P. (2001). Temporal and spatial patterns of zooplankton in the chesapeake bay turbidity maximum. *Marine Ecology Progress Series*, 213:215–227.

[Rousselet et al., 2018] Rousselet, L., De Verneil, A., Doglioli, A. M., Petrenko, A. A., Duhamel, S., Maes, C., and Blanke, B. (2018). Large-to submesoscale surface circulation and its implications on biogeochemical/biological horizontal distributions during the outpace cruise (southwest pacific). *Biogeosciences*, 15(8).

[Rudnick and Klinke, 2007] Rudnick, D. L. and Klinke, J. (2007). The Underway Conductivity Temperature Depth Instrument. *Journal of Atmospheric and Oceanic Technology*, 24:1910–1923.

[Scalabrin et al., 2009] Scalabrin, C., Marfia, C., and Boucher, J. (2009). How much fish is hidden in the surface and bottom acoustic blind zones? *ICES J. Mar. Sci.*, 66.

[Siegelman et al., 2019] Siegelman, L., O'toole, M., Flexas, M., Rivière, P., and Klein, P. (2019). Submesoscale ocean fronts act as biological hotspot for southern elephant seal. *Scientific reports*, 9(1):1–13.

[Simmonds and MacLennan, 2008] Simmonds, J. and MacLennan, D. N. (2008). *Fisheries acoustics: theory and practice*. John Wiley and Sons.

[Sinclair and Stabeno, 2002] Sinclair, E. and Stabeno, P. (2002). Mesopelagic nekton and associated physics of the southeastern bering sea. *Deep Sea Research Part II: Topical Studies in Oceanography*, 49(26):6127–6145.

[St John et al., 2016] St John, M. A., Borja, A., Chust, G., Heath, M., Grigorov, I., Mariani, P., Martin, A. P., and Santos, R. S. (2016). A dark hole in our understanding of marine ecosystems and their services: perspectives from the mesopelagic community. *Frontiers in Marine Science*, 3:31.

[Stanton et al., 2018] Stanton, T. K., Lee, W.-J., and Baik, K. (2018). Echo statistics associated with discrete scatterers: A tutorial on physics-based methods. *The Journal of the Acoustical Society of America*, 144(6):3124–3171.

[Suberg et al., 2014] Suberg, L., Wynn, R. B., Van Der Kooij, J., Fernand, L., Fielding, S., Guihen, D., Gillespie, D., Johnson, M., Gkikopoulou, K. C., Allan, I. J., et al. (2014). Assessing the potential of autonomous submarine gliders for ecosystem monitoring across multiple trophic levels (plankton to cetaceans) and pollutants in shallow shelf seas. *Methods in Oceanography*, 10:70–89.

[Sundermeyer and Ledwell, 2001] Sundermeyer, M. A. and Ledwell, J. R. (2001). Lateral dispersion over the continental shelf: Analysis of dye release experiments. *Journal of Geophysical Research: Oceans*, 106(C5):9603–9621.

[Sutton et al., 2017] Sutton, T. T., Clark, M. R., Dunn, D. C., Halpin, P. N., Rogers, A. D., Guinotte, J., Bograd, S. J., Angel, M. V., Perez, J. A. A., Wishner, K., et al. (2017). A global biogeographic classification of the mesopelagic zone. *Deep Sea Research Part I: Oceanographic Research Papers*, 126:85–102.

[Underwood et al., 2020] Underwood, M. J., García-Seoane, E., Klevjer, T., Macaulay, G. J., and Melle, W. (2020). An acoustic method to observe the distribution and behaviour of mesopelagic organisms in front of a trawl. *Deep Sea Research Part II: Topical Studies in Oceanography*, page 104873.

[Wiebe et al., 1992] Wiebe, P. H., Copley, N. J., and Boyd, S. H. (1992). Coarse-scale horizontal patchiness and vertical migration of zooplankton in gulf stream warm-core ring 82-h. *Deep Sea Research Part A. Oceanographic Research Papers*, 39:S247–S278.

[Wiebe et al., 2002] Wiebe, P. H., Stanton, T. K., Greene, C. H., Benfield, M. C., Sosik, H. M., Austin, T. C., Warren, J. D., and Hammar, T. (2002). Biomaper-ii: an integrated instrument platform for coupled biological and physical measurements in coastal and oceanic regimes. *IEEE Journal of Oceanic Engineering*, 27(3):700–716.

[Wishner et al., 2013] Wishner, K. F., Outram, D. M., Seibel, B. A., Daly, K. L., and Williams, R. L. (2013). Zooplankton in the eastern tropical north pacific: Boundary effects of oxygen minimum zone expansion. *Deep Sea Research Part I: Oceanographic Research Papers*, 79:122–140.

[Wishner et al., 2018] Wishner, K. F., Seibel, B. A., Roman, C., Deutsch, C., Outram, D., Shaw, C. T., Birk, M. A., Mislan, K. A. S., Adams, T. J., Moore, D., and Riley, S. (2018). Ocean deoxygenation and zooplankton: Very small oxygen differences matter. *Science Advances*, 4(12).

[Yamamoto and Nishizawa, 1986] Yamamoto, T. and Nishizawa, S. (1986). Small-scale zooplankton aggregations at the front of a kuroshio warm-core ring. *Deep Sea Research Part A. Oceanographic Research Papers*, 33(11-12):1729–1740.

8 Supplemental Information

8.1 Model Side-Looking Echosounder Pings

A 3D echosounder simulation was constructed to examine the received backscatter signal from a horizontally insonified scattering layer. The received power and Scattering Volume (Sv) were calculated by solving the sonar equation across a conical acoustic beam extending 100m in range. The received sound intensity level (RL) was calculated for range and angle cells as a function of the source level (SL) and target strength (TS) for backscatter targets after accounting for the two-way spreading and absorption transmission loss (TL) terms. To simulate the beam pattern affect, a loss term was added to achieve a 3db reduction in power at half of the beam width. The received signal was scaled by the volume of each range angle cell to approximate the total contribution of scatterers that would be uniformly distributed in the cell. The total power was calculated by summing the received sound intensity level RL across angle cells in the linear domain. A noise term (NL) was added to the received signal power in the linear domain to simulate stationary additive noise at the transducer. The Scattering Volume was calculated by normalizing the received power by the beam area at range.

Beam simulator pseudo code:

for i=1:dRange:Range
  for j = 0:dTheta:Theta/2
    RL (i, j) = $10\hat{}$[(SL(angle) -TL(range) + TS(angle, range))10]
    RL (i, j) = RL * Beam Sector Volume(i,j)
  end
  Received Power(i) = 10*log10[Sum RL(i) + $10\hat{}$(NL/10)]
  Scattering Volume = Received Power(i) / Beam Sector Volume(i)
End

We simulated the received backscatter signal from insonified 'high' and 'low' TS horizontal layers, reflecting the scattering conditions within or outside the scattering layer from the side-looking perspective (Figure 15). The model results show that when a sonar system is not noise limited over the 100 meter acoustic range (i.e. NL < SL + TS - TL for all ranges), there is a fixed offset between the power for the high and low TS pings equal to the delta TS between the scattering environments (Figure 16). When the system is noise limited before 100 meters due to the transmission loss (NL > SL + TS - TL), the offset between the power for the high and low TS pings is not fixed over range and reflects instead a convergence to the noise floor affected by the spreading loss, and the power difference between the high and low TS layer signal decays logarithmically.

These model results reflect what is seen in the side-looking Wire Flyer data when the data is 'detrended' over range, by subtracting an approximated average return (Figure 17). For high intensity pings recorded at the scattering layers, the detrended data reveals the signal at a maximum (scaled to the scattering layer TS) near the transducer and dropping towards the noise floor as a function of the TL terms. For this reason, excess signal strength for homogenous scattering

layers is obtained over range until the SNR reaches 0, and thus higher intensity scattering layers result in a detectable signal over farther ranges than in weaker scattering layers. This also explains related phenomenon seen in the Wire Flyer datasets, such as scattering layers recorded before installation of an input power filter (higher NL) being detectable over shorter ranges than in the input power filtered (lower NL) data.

The simulated power approximated the overall trends observed in the real Wire Flyer Power data, but we were unable to match the slopes exactly at both short and long ranges. More sophisticated modeling efforts may provide an ability to quantify increased signal extinction due to enhanced scattering losses from the side-looking perspective, a phenomenon we imagine is likely to affect the acoustic recordings.

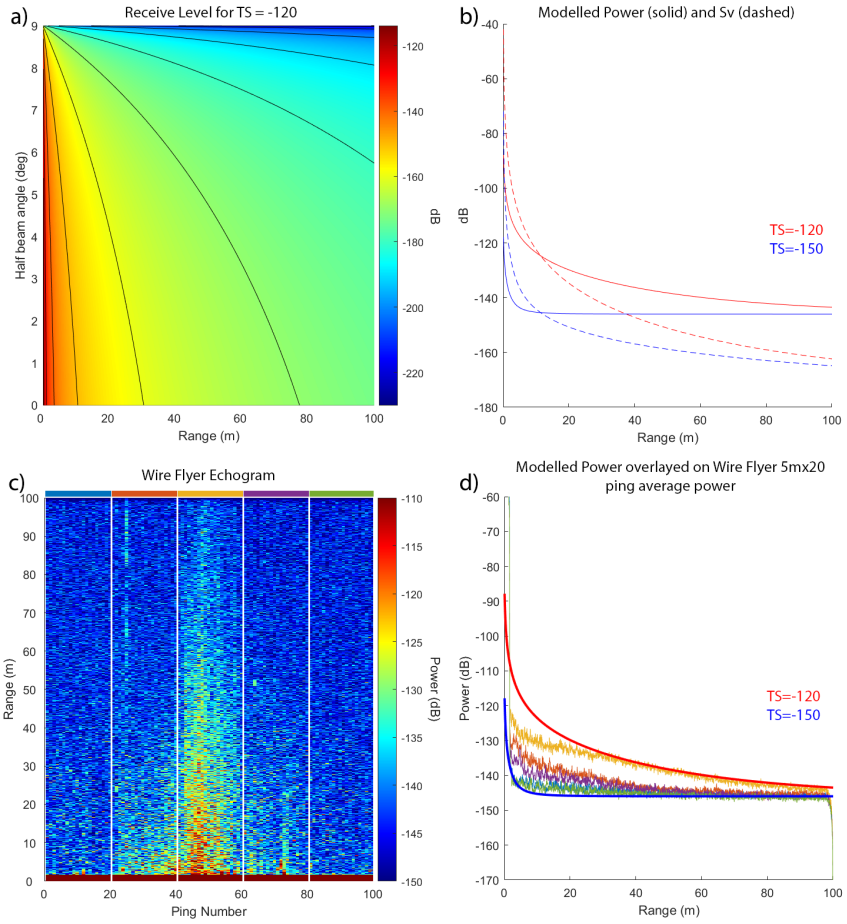

Figure 15: Simulated side-looking echosounder Power and Sv data (Theta = 18 deg, SL = 15 dB, NL=-146 dB, AbsCo=20 dB/km) matches the Wire Flyer data. A) Receive level distribution for a homogeneous scattering layer of -120 dB Target Strength across range angle cells. B) Modelled Power and Sv ping data for scattering layers of -120 and -150 dB Target Strength. C) Wire Flyer 100 ping power echogram showing bounded scattering feature. The colored bars atop show the 20 pings averaged for comparison to the model power data. D) Simulated power pings for TS=-120 dB and TS=-150 dB overlaid on Wire Flyer 20 ping power averages showing good alignment at far ranges.

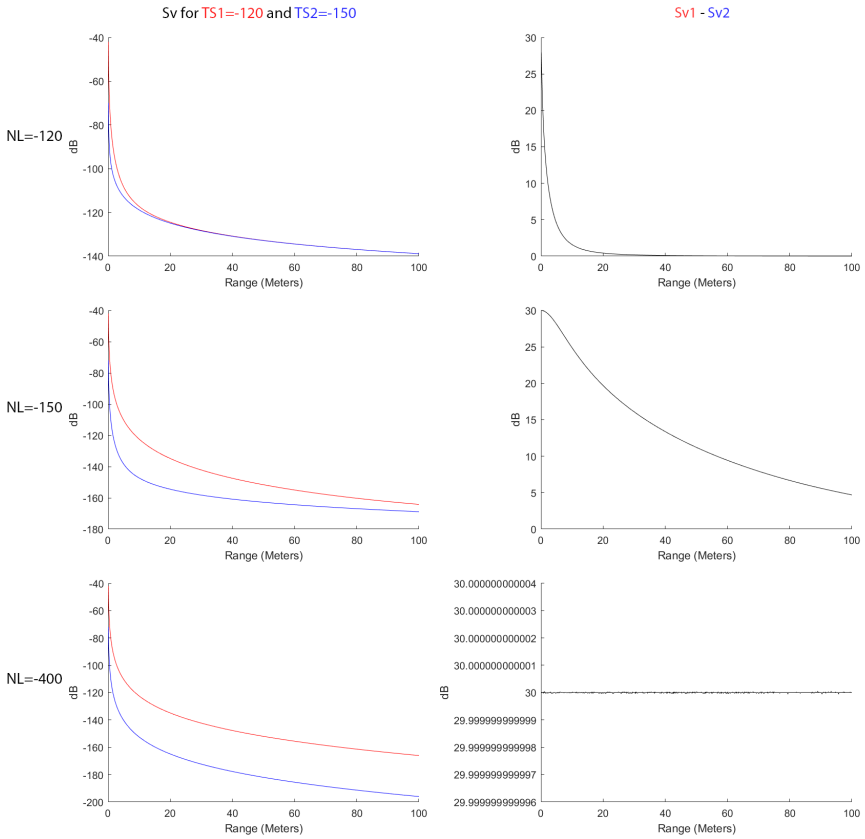

Figure 16: Modelled Scattering Volume for two scattering layers with TS=-120 and TS=-150 dB on the left panels, and the difference between the Sv for the high minus low TS pings on the right panel, under increasing Noise Levels (-120 dB top row, -150 dB middle row, -400 dB bottom row).

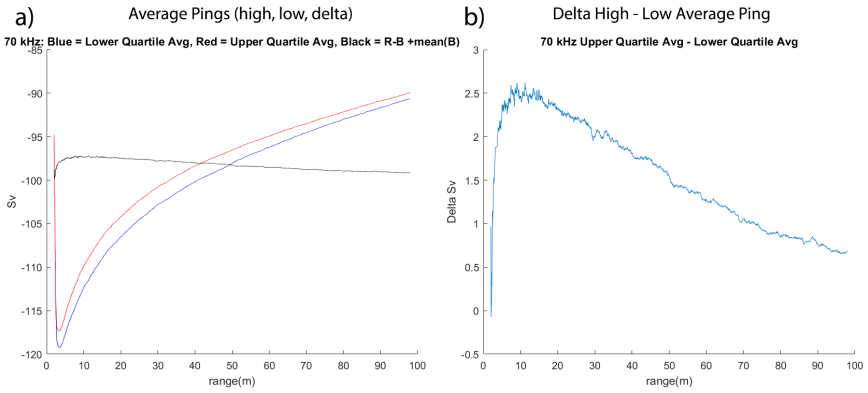

Figure 17: Averaged Wire Flyer Sv data from the Baltimore Canyon deployment demonstrating the raw and detrended Sv curves over range. A) Averaged 0-25% (blue) and 75-100% (red) Sv quartile averages. The difference between the high and low quantiles with an average value added back is shown in black and represents the detrended Sv data. B) The raw difference between the upper and lower Sv quantiles matches the logarithmic decay observed in the simulated Sv data.